

Study on the distribution law of stress deviator below the floor of a goaf

Zhaolong Li^{*1}, Renliang Shan^{1a}, Chunhe Wang^{1,2a}, Honghu Yuan^{1b} and Yonghui Wei^{1b}

¹School of Mechanics and Civil Engineering, China University of Mining & Technology (Beijing), Beijing 100083, China

²China Construction Communications Engineering Group Corporation Limited, Beijing 100161, China

(Received February 7, 2020, Revised March 19, 2020, Accepted March 25, 2020)

Abstract. In the process of mining closely spaced coal seams, the problem of roadway arrangement in lower coal seams has long been a concern. By means of mechanical model calculation and numerical simulation postprocessing, the distribution of the stress deviator below the floor of a goaf and the evolution of the stress deviator in the vertical and horizontal directions are studied under the influence of horizontal stress. The results of this theoretical study and numerical simulation show that the stress deviator decreases exponentially with increasing depth from the floor below the coal side. With the increase in the horizontal stress coefficient λ , the stress deviator concentration area shifts. The stress deviator is concentrated within 10 m below the goaf and 15 m laterally from the coal side; thus, the magnitude of the surrounding rock stress deviator should be considered when planning the construction of a roadway in this area.

Keywords: closely spaced coal seams; roadway layout; stress deviator; horizontal stress

1. Introduction

China has abundant reserves of closely spaced coal seams, and downward mining is the most common method used to mine closely spaced coal seams. When mining of the upper seam is completed, the damage to the floor of the caved zone affects the strength of the rock surrounding the lower coal seam. The residual coal pillars transmit the overburden pressure to the floor (Suchowerska *et al.* 2013), resulting in a concentration of the abutment pressure in the floor near the coal pillar, which seriously affects the stability of the rock surrounding the lower coal seam. Many factors, such as the bearing capacity of the coal pillars (Chen *et al.* 2018), the mechanical characteristics of the surrounding rocks, and the pattern of stress transmission, determine the stress state of the surrounding rocks below the floor. Therefore, when mining closely spaced coal seams (Tan *et al.* 2010, Brady *et al.* 1993), the stability of the roadway in the lower coal seam is complex and affected by many factors (Fu *et al.* 2018). The reasonable selection of roadway support technology and roadway position is the key to ensuring roadway stability.

Roadway stability in longwall coal mining is critical (Mahdevari 2017). Many scholars worldwide have carried out various studies on the stability of roadways (Chen *et al.* 2016, Toraño *et al.* 2002, Majcherczyk *et al.* 2014). Some studies have made great contributions to the prediction of convergence in tunnels (Mahdevari 2013) and the stability of the coalface (Mahdevari *et al.* 2016). Yuan *et al.* (2018)

studied roadway support technology under the influence of mining. It is undeniable that reasonably selecting the position of a roadway in a lower coal seam based on consideration of the stress distribution in the surrounding rock (Das *et al.* 2019, Widisinghe *et al.* 2014, Marino *et al.* 2012, Sivakugan *et al.* 2014) is critical to the safety of the roadway. Yan *et al.* (2015) through numerical simulation, determined a reasonable roadway position and support parameters. Zhu *et al.* (2017) established a mechanical model of the stress distribution below a goaf and derived the horizontal and vertical stress equations for the floor. Shang *et al.* (2019) suggested that a roadway below an isolated residual coal pillar in the upper coal seam should be avoided when mining in such conditions. Liu *et al.* (2016) used UDEC to reveal the stress state of the surrounding rock near the goaf and proposed that the location of a lower coal seam roadway should avoid stress concentration areas. In addition, Li *et al.* (2016) effectively controlled the occurrence of rock bursts and other events by staggering the arrangement of roadways.

Previous research on this topic focused on the concentration of vertical stress below the floor of the goaf. However, there are also horizontal stresses, shear stresses and stress deviators that determine the stress state of the surrounding rocks in the floor. In recent years, research on stress deviators has made some progress through theoretical advancements (Jiang *et al.* 2004, Martin Kroon *et al.* 2013), calculations (Bernasconi 2002), and experiments (Lockner 2002, Zhao *et al.* 2020, Wang *et al.* 2012). However, in earlier studies of geology and mining, there was relatively little exploration of the stress deviator. In elastic-plastic mechanics, it is proposed that the inelastic deformation of a rock mass is usually caused by the stress deviator. The second invariant J_2 of the stress deviator can represent the distortion energy density of the rock mass and can directly affect the stability of the surrounding rock. Some scholars

*Corresponding author, Ph.D. Student
E-mail: cumtblzl@163.com

^aProfessor

^bPh.D. Student

(Wang *et al.* 2017, Sun *et al.* 2016) have made progress in the study of the stress deviator in the surrounding rock near a goaf. He *et al.* (2014) studied the variation in the stress deviator around a roadway. Therefore, it is of great significance to study the distribution pattern of the stress deviator in an upper coal seam floor with different horizontal stress conditions in the mining process.

2. Project summary

2.1 Geological condition

The Malan Mine is located 50 km west of Taiyuan city, Shanxi Province, China and is a high-gas mine. To ensure the safe mining of the coal seams, a number of gas drainage roadways (Krause 2009, Cao *et al.* 2018) have been excavated in the mine.

The main coal seams currently being mined in the Malan Mine are the #02 and #2 coal seams, with average thicknesses of 2.14 m and 2.20 m, respectively, and the coal seams have inclination angles of 1-9°. The distance between the two coal seams is approximately 7 m, and the intervening rock is composed mostly of mudstone and fine sandstone. The immediate roof of the #02 coal seam

is a 6.05 m thick silty mudstone, and the immediate floor of the #2 coal seam is a 2 m thick siltstone. The Malan Mine is a typical coal mine with closely spaced coal seams; a columnar section of the strata is shown in Fig. 1.

2.2 Longwall panel arrangement and mining sequence

The 10606 longwall panel is located in the sixth mining district of the Malan Mine and mines the #02 coal seam at an average burial depth of 400 m. After mining of the 10606 panel, the mine plans to position the 10608 gas drainage roadway in the #2 coal seam to extract gas from the 10608 longwall panel, the 10606 goaf and #2 coal seam near the roadway area to ensure safe mining. Additionally, the 10608 gas drainage roadway will be used as the gate roadway for the later stage of mining of the #2 coal seam. The layout of the longwall panel is shown in Fig. 2. The boundary between the goaf and the coal pillar is called the coal side.

The multiple functions of the gas drainage roadway highlight the importance of the safety and stability of the roadway. During the mining of the upper coal seam, instability in the gas drainage roadway will cause security incidents (Mahdevari *et al.* 2014) and have a great impact on the panel layout of the lower coal seam. After the completion of the gas drainage roadway, it is mainly affected by the concentrated stress on the side of the 10606 goaf. The stress concentration has different effects on the stress environment of the surrounding rock in different areas below the goaf. Therefore, reasonable selection of the location of the gas drainage roadway is a prerequisite to ensure the stability of the roadway and maximize the utilization of resources.

3. Theoretical calculation of the stress deviator below the floor

According to the theory of mine pressure, after the #2 coal seam is mined, considerable asymmetry will exist in the floor stress below the mined-out area and below the coal pillars. Many scholars (Singh *et al.* 2011, Sun *et al.* 2019, Jaouhar *et al.* 2018, Zhao *et al.* 2000) have theoretically calculated the additional stress caused by mining. The nonuniform distribution of stress will change the stress deviator in the surrounding rock of the floor, which may cause deformation and failure of the surrounding rock. In this section, the second invariant J_2 of the stress deviator of the coal seam floor is calculated theoretically throughout the mining process to provide a theoretical basis for guiding the rational layout of the roadway below a coal pillar.

3.1 Calculation of the stress deviator second invariant

J_2

In elastic-plastic mechanics, the stress tensor σ_{ij} can be decomposed into two parts: the spherical stress tensor $\sigma_0\delta_{ij}$ and the stress deviator s_{ij} . The deformation corresponding to the former is generally elastic deformation, while the inelastic deformation of a material is mainly caused by the stress deviator.

Thickness/m	Lithology	Strata	Rock features
6.05		Silty mudstone	Dark gray, thickly layered
2.14		#02 Coal	Black, lumpy, poor lithology
4.97		Sandstone	Off-white medium-fine sandstone, mainly quartz and feldspar
0.45		#1 Coal	Black, containing sandy mudstone
1.49		Silty mudstone	Dark gray, containing pyrite film
2.20		#2 Coal	Black, semibright coal, blocky
1.89		Siltstone	Gray, containing fossilized plant roots
0.49		#3 Coal	Black, semibright coal, blocky
5.00		Silty mudstone	Dark grey

Fig. 1 Columnar section of the rock strata

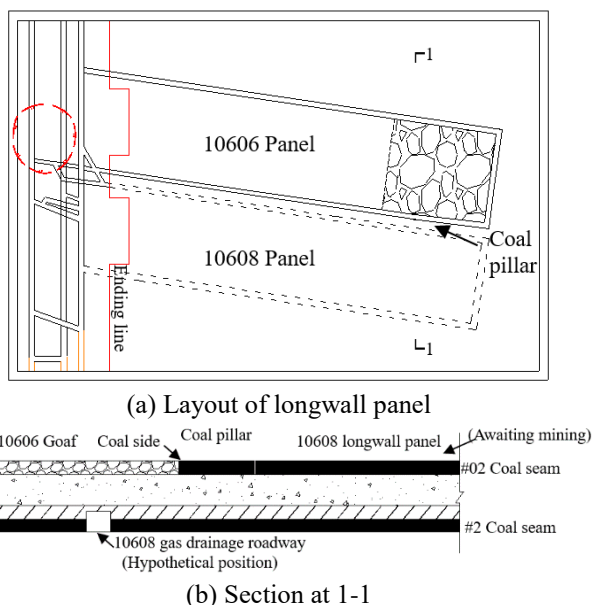


Fig. 2 Arrangement of the longwall panel

$$\sigma_{ij} = \sigma_0 \delta_{ij} + s_{ij} = \begin{bmatrix} \sigma_x & \tau_{xy} & \tau_{xz} \\ \tau_{yx} & \sigma_y & \tau_{yz} \\ \tau_{zx} & \tau_{zy} & \sigma_z \end{bmatrix} \quad (1)$$

$$\sigma_0 = (\sigma_1 + \sigma_2 + \sigma_3) / 3$$

$$\delta_{ij}(i, j = x, y, z) = \begin{cases} 1 & (i = j) \\ 0 & (i \neq j) \end{cases}$$

The stress deviator s_{ij} is a symmetrical second-order tensor with three principal values, s_1 , s_2 , and s_3 .

$$s_{ij} = \begin{bmatrix} \sigma_1 - \sigma_0 & 0 & 0 \\ 0 & \sigma_2 - \sigma_0 & 0 \\ 0 & 0 & \sigma_3 - \sigma_0 \end{bmatrix} = \begin{bmatrix} s_1 & 0 & 0 \\ 0 & s_2 & 0 \\ 0 & 0 & s_3 \end{bmatrix} \quad (2)$$

$$s_i = \sigma_i - \sigma_0 \quad (i=1,2,3)$$

The second invariant J_2 of the stress deviator is often used in elastic-plastic mechanics, and the stability state of the rock mass can be judged according to the value of J_2 . Therefore, this paper uses the second invariant J_2 of the stress deviator to characterize the stress deviator of the coal and rock in the floor, providing a basis for the selection of the location of the gas drainage roadway below the floor of the goaf.

$$J_2 = \frac{s_1^2 + s_2^2 + s_3^2}{2} = \frac{[(\sigma_1 - \sigma_2)^2 + (\sigma_2 - \sigma_3)^2 + (\sigma_3 - \sigma_1)^2]}{6} \quad (3)$$

In Eq. (3), J_2 represents the deviation between the actual stress state and the average stress state of the rock mass. The larger J_2 is, the greater the distortion energy density and shear stress of the surrounding rock, that is, the worse the stability of the surrounding rock.

3.2 Stress deviator distribution in the floor below the goaf

According to the distribution of mine pressure (Brady *et al.* 1993) and the distribution of vertical stress near the goaf (Yavuz 2004), when the mining of the 10606 panel is completed, the surrounding rock of the floor can be regarded as a semi-infinite ideal elastomer (Zhang *et al.* 2018), and the lateral abutment pressure increment on the

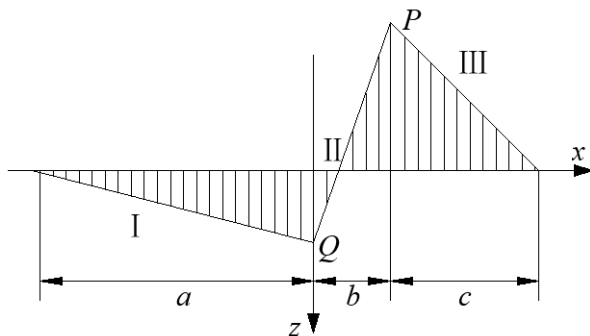


Fig. 3 Calculation model of the additional stress in the floor below the goaf

side of the 10606 goaf can be simplified (Suchowska *et al.* 2013, Zhang *et al.* 2018), as shown in Fig. 3.

In Fig. 3, P is the maximum value ($K\gamma H - \gamma H$) of the additional stress in the floor below the coal, Q is the maximum value ($-\gamma H$) of the additional stress in the floor below the goaf, a is the influence range of the additional stress below the goaf, b is the distance between the peak of the support pressure and the coal side, and c is the length of the elastic deformation zone. K is the maximum stress concentration coefficient, γ is the volume weight of the overburden, H is the mining depth. According to the principle of force balance, the additional stress should conform to formula (4):

$$\left(\frac{b}{K} + a\right) \cdot Q + \left(\frac{K-1}{K} \cdot b + c\right) \cdot P = 0 \quad (4)$$

According to the theory of elastic mechanics, the effect of an additional stress on any point M in the floor can be obtained by integrating the microconcentrated force dt of the additional stress at t .

$$\sigma'_z = -\frac{2}{\pi} \int_{-a}^{b+c} \frac{q(t)z^3 dt}{[(x-t)^2 + z^2]^{\frac{5}{2}}}$$

$$\sigma'_x = -\frac{2}{\pi} \int_{-a}^{b+c} \frac{q(t)z(x-t)^2 dt}{[(x-t)^2 + z^2]^{\frac{5}{2}}} \quad (5)$$

$$\tau'_{xz} = -\frac{2}{\pi} \int_{-a}^{b+c} \frac{q(t)z^2(x-t) dt}{[(x-t)^2 + z^2]^{\frac{5}{2}}}$$

In Eq. (5), σ'_z , σ'_x and τ'_{xz} represent the vertical, horizontal and shear stresses caused by the additional stress at point M in the floor, respectively.

Eq. (5) is used to calculate the additional stress at M , which is induced by the downward transfer of the abutment pressure in areas I, II, and III. The stress state at any point below the floor of the goaf can be obtained by superposing the stress of each region on point M .

The additional stress in the surrounding rock of the floor caused by area I is:

$$\sigma'_{z1} = \left(\frac{\gamma H x}{\pi a} + \frac{\gamma H}{\pi}\right) \left[\frac{xz}{x^2 + z^2} - \frac{(x+a)z}{(x+a)^2 + z^2} + \arctan \frac{x}{z} - \arctan \frac{x+a}{z} \right]$$

$$\sigma'_{x1} = \left(\frac{\gamma H x}{\pi a} + \frac{\gamma H}{\pi}\right) \left[\frac{(x+a)z}{(x+a)^2 + z^2} - \frac{xz}{x^2 + z^2} + \arctan \frac{x}{z} - \arctan \frac{x+a}{z} \right] \quad (6)$$

$$\tau'_{xz1} = \left(\frac{\gamma H x}{\pi a} + \frac{\gamma H}{\pi}\right) \left[\frac{z^2}{(x+a)^2 + z^2} - \frac{z^2}{x^2 + z^2} \right]$$

The additional stress in the surrounding rock of the floor caused by area II is:

$$\sigma'_{z2} = \left(\frac{\gamma H}{\pi} - \frac{K\gamma H x}{\pi b}\right) \left[\frac{(x-b)z}{(x-b)^2 + z^2} - \frac{xz}{x^2 + z^2} + \arctan \frac{x-b}{z} - \arctan \frac{x}{z} \right]$$

$$\sigma'_{x2} = \left(\frac{\gamma H}{\pi} - \frac{K\gamma H x}{\pi b}\right) \left[\frac{xz}{x^2 + z^2} - \frac{(x-b)z}{(x-b)^2 + z^2} + \arctan \frac{x-b}{z} - \arctan \frac{x}{z} \right] \quad (7)$$

$$\tau'_{xz2} = \left(\frac{K\gamma H x}{\pi b} - \frac{\gamma H}{\pi}\right) \left[\frac{z^2}{(x-b)^2 + z^2} - \frac{z^2}{x^2 + z^2} \right]$$

The additional stress in the surrounding rock of the floor

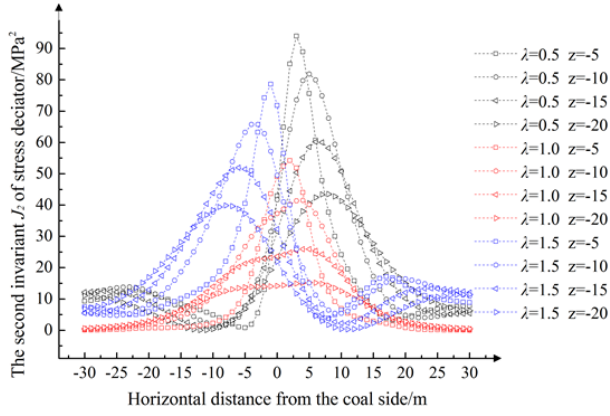


Fig. 4 Theoretical stress deviator

caused by area III is:

$$\begin{aligned}\sigma'_{z3} &= \left[(1-K) \frac{b+c-x}{\pi c} \gamma H \right] \times \left[\frac{(x-b-c)z}{(x-b-c)^2+z^2} - \frac{(x-b)z}{(x-b)^2+z^2} \right. \\ &\quad \left. + \arctan \frac{x-b-c}{z} - \arctan \frac{x-b}{z} \right] \\ \sigma'_{x3} &= \left[(1-K) \frac{b+c-x}{\pi c} \gamma H \right] \times \left[\frac{(x-b)z}{(x-b)^2+z^2} - \frac{(x-b-c)z}{(x-b-c)^2+z^2} \right. \\ &\quad \left. + \arctan \frac{x-b-c}{z} - \arctan \frac{x-b}{z} \right] \\ \tau'_{xz3} &= \left[(K-1) \frac{b+c-x}{\pi c} \gamma H \right] \times \left[\frac{z^2}{(x-b-c)^2+z^2} - \frac{z^2}{(x-b)^2+z^2} \right]\end{aligned}\quad (8)$$

Here, λ is the horizontal stress coefficient. By superimposing the additional stress at point M with the original stress, the stress state at point M can be obtained.

$$\begin{aligned}\sigma_z &= \sigma'_{z1} + \sigma'_{z2} + \sigma'_{z3} + \gamma H \\ \sigma_x &= \sigma'_{x1} + \sigma'_{x2} + \sigma'_{x3} + \lambda \gamma H \\ \tau_{xz} &= \tau'_{xz1} + \tau'_{xz2} + \tau'_{xz3}\end{aligned}\quad (9)$$

According to Mohr-Coulomb theory, if there is only normal stress and no shear stress on a certain inclined plane, this inclined plane is called the principal plane, the corresponding normal stress is called the principal stress, and the corresponding direction is called the principal direction. To simplify the calculation, the stress in the y direction is regarded as the second principal stress with the same value as the stress in the x direction. Then, the principal stress at any point below the floor of the goaf can be expressed as:

$$\begin{aligned}\sigma_1 &= \frac{\sigma_x + \sigma_z}{2} + \sqrt{\left(\frac{\sigma_x - \sigma_z}{2}\right)^2 + \tau_{xz}^2} \\ \sigma_2 &= \sigma_x = \sigma_x + \lambda \gamma H \\ \sigma_3 &= \frac{\sigma_x + \sigma_z}{2} - \sqrt{\left(\frac{\sigma_x - \sigma_z}{2}\right)^2 + \tau_{xz}^2}\end{aligned}\quad (10)$$

Eqs. (9) and (10) indicate that the horizontal stress coefficient λ is an important condition that affects the stress

deviator. According to Malan Mine data, we substitute the values $a=21.8$ m, $b=2$ m, $c=15$ m, and $K=2.4$ into the above formula and calculate the stress deviator of the floor when $\lambda = 0.5, 1,$ and 1.5 . The values conform to formula (4). The calculation results are shown in Fig. 4.

Fig. 4 shows the following: ① The peak value of the stress deviator and the concentration area appear in the rock mass below the coal side. When λ is constant, the stress deviator of the floor decreases with increasing depth. ② As λ increases, the position of the peak value and concentration area of the stress deviator gradually rotate from the rock below the solid coal to the rock below the coal side and the goaf. ③ With the increase in $|\lambda|$, the stress deviator of the floor increases.

4. Distribution law of the stress deviator in the floor

4.1 The numerical model

To study the stress deviator distribution in the surrounding rock below the goaf, we employed Flac3D software to establish a numerical model based on the characteristics of the rock strata in the Malan Mine.

The model size is $x \times y \times z = 200$ m \times 20 m \times 50 m, with lateral hinged support and bottom fixed support. A total of 100000 zones and 112761 grids were applied. The range $0 < x < 90$ in the #02 coal seam represents the 10606 panel. The simulated depth of the model was 400 m, and a uniform load of 400×0.25 MPa was applied to the top of the model. The coal and rock mass in the model obeys the Mohr-Coulomb yield criterion (Shan *et al.* 2013, Cui 2017). The selected horizontal stress coefficients were 0.5, 0.8, 1.0, 1.2 and 1.5, and the initial equilibrium calculation stopped when the preset parameter (mech ratio $1e-5$) was reached.

To obtain the mechanical parameters of the surrounding rocks, rock samples were taken from the site. Triaxial compression and tensile tests of the rock samples were carried out in a rock mechanics laboratory using a DRTS-500 rock triaxial compression test system and rock tensile testing machine (Fig. 6). The cohesion, friction angle, Young's modulus and Poisson's ratio of the rock were obtained through triaxial compression experiments. The bulk modulus and shear modulus of the rock were calculated based on the Young's modulus and Poisson's ratio values. The tensile strength was obtained through tensile tests. The rock mechanical parameters are shown in Table 1.

4.2 The stress deviator distribution law in the floor after mining is completed

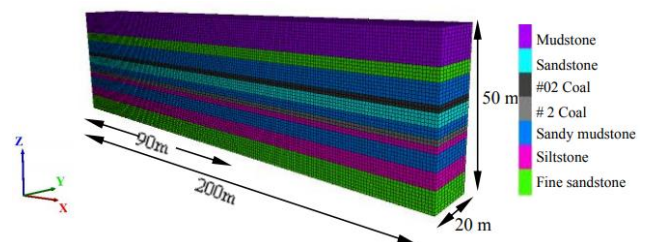


Fig. 5 The numerical model

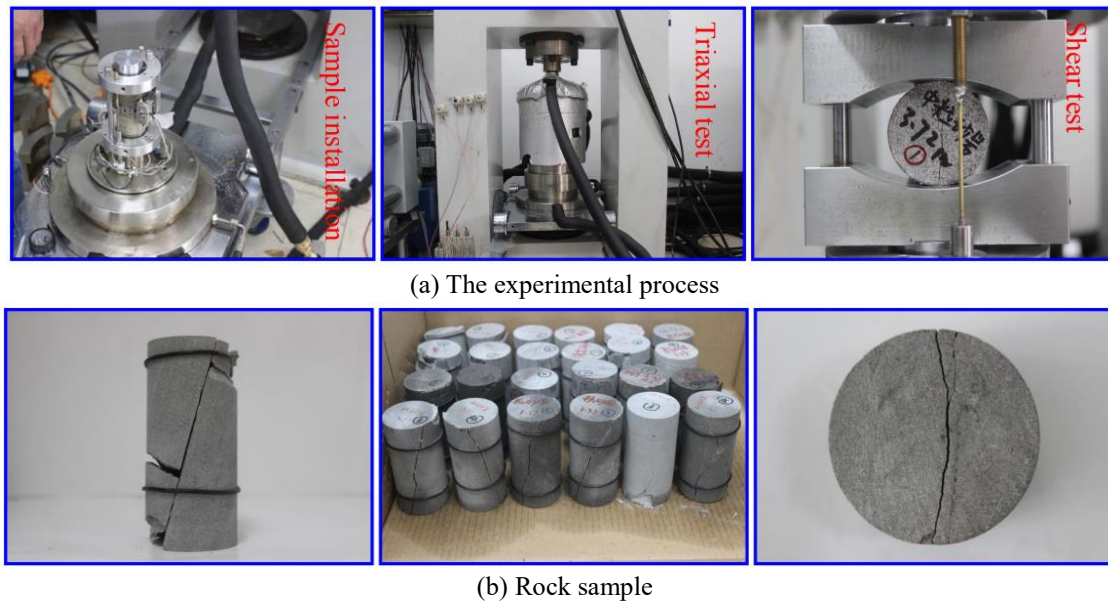


Fig. 6 Mechanical property tests

Table 1 Mechanical parameters of the rock strata

Rock formation	Bulk modulus (GPa)	Shear modulus (GPa)	Density (kg·m ⁻³)	Friction angle (°)	Cohesion (MPa)	Tensile strength (MPa)
Sandy mudstone	3.8	2.6	2350	32	3.3	2.4
Fine sandstone	11.3	6.8	2500	34	3.1	2.7
Mudstone	3.6	2.1	2300	32	2.3	2.2
Sandstone	9.2	3.2	2400	32	2.6	2.3
Coal	1.3	1.1	1600	28	1.8	0.75
Siltstone	13.3	10.8	2600	35	4.9	2.9

Following excavation of the 10606 panel and reestablishment of equilibrium, the stress data of the surrounding rock in the model was extracted. Then, after this formula-based calculation, the distribution of the stress deviator below the goaf was plotted using Origin software for horizontal stress coefficients of $\lambda = 0.5, 0.8, 1.0, 1.2,$ and 1.5 .

As shown in Fig. 7, (1) the peak of the stress deviator in the floor appears in the rock mass below the coal side, and the stress deviator decreases rapidly with an increase in depth. The location of the new roadway should be in the area where the stress deviator is low. (2) With an increase in λ , the stress deviator concentration area shifts. When $\lambda \leq 1$, the stress deviator concentration area is located in the rock mass below the solid coal. At this time, attention should be paid to the selection of coal pillar width to avoid excessive stress deviator values in the coal pillar area. When $\lambda > 1$, the stress deviator concentration area is located in the rock mass below the goaf. At this time, to avoid the danger of excavating the roadway in the stress deviator concentration area, the distance between the coal side and the lower coal seam roadway should be increased. (3) As λ approaches 1.0, the range of the stress deviator concentration area is small, and as $|1-\lambda|$ increases, this range increases significantly. The simulation results are basically consistent with the theoretical calculation results.

4.3 The rotation of the stress deviator concentration area

This section extracts the locations and values of the peak stress deviator at various depths with different horizontal stress coefficients to more intuitively show the rotation of the stress deviator concentration area with the change in λ , as shown in Fig. 8.

Fig. 8 illustrates the following findings: (1) When $\lambda \leq 1$, the stress deviator decreases exponentially along the direction of the peak axis of the stress deviator in the floor, and the peak axis of the stress deviator is at an angle of 30° to the vertical axis. As the depth increases, the angle between the peak axis of the stress deviator and the vertical axis decreases gradually, and the rate of reduction in the stress deviator decreases gradually. (2) When $\lambda > 1$, the stress deviator decreases exponentially along the peak axis at an angle of -45° from the vertical direction. With increasing depth, the angle between the peak axis of the stress deviator and the vertical axis decreases, and the rate of reduction in the stress deviator decreases gradually. The rate of reduction in the stress deviator at $\lambda > 1$ is lower than that at $\lambda \leq 1$.

This section studies the stress deviator of each rock layer below the floor when $\lambda = 0.5, 1.0,$ and 1.5 and analyzes the influence of the horizontal stress coefficient λ and depth z on the stress deviator distribution of the rock

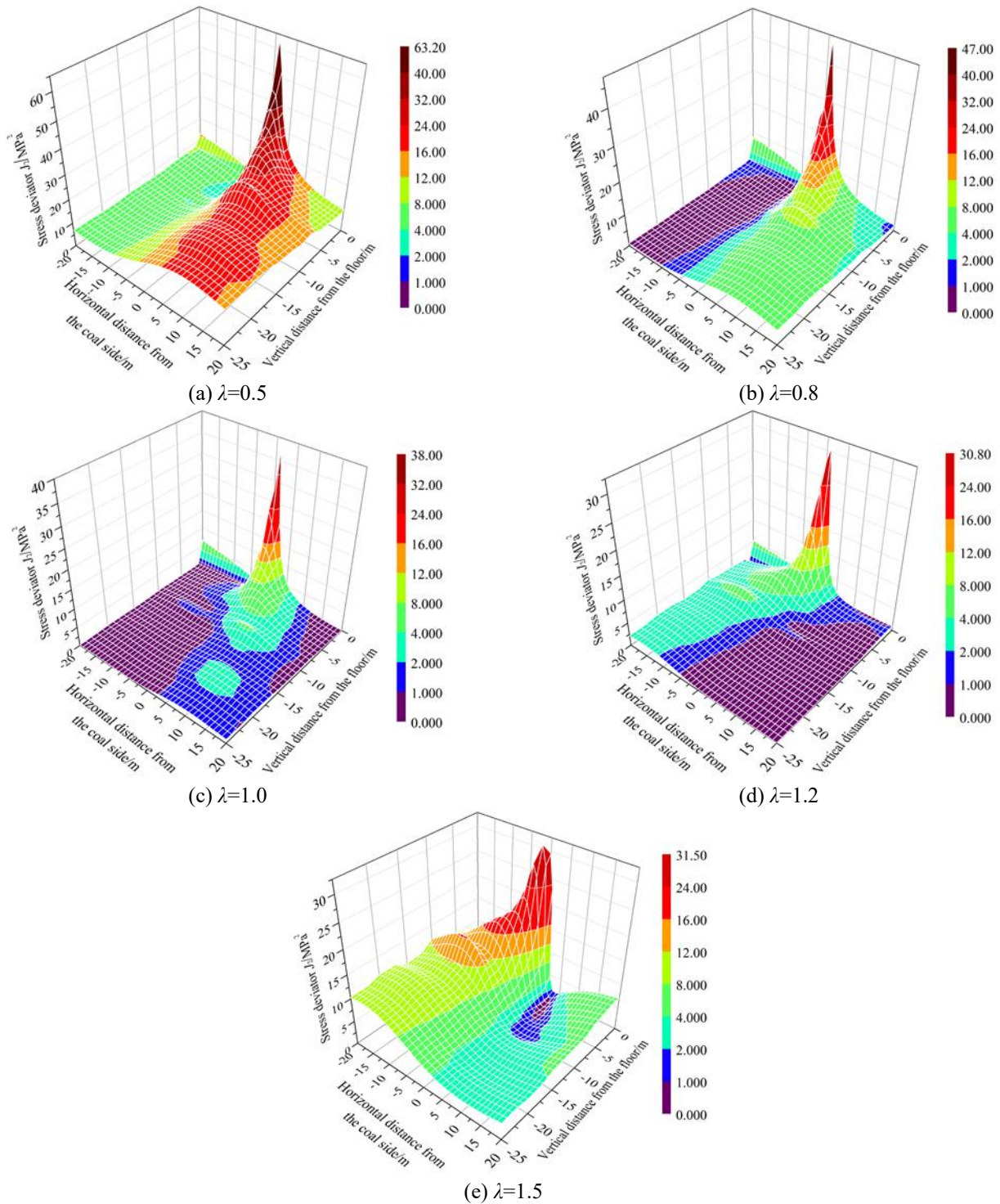


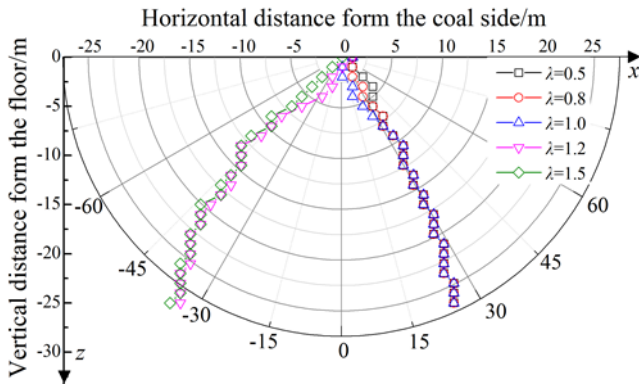
Fig. 7 Stress deviator distribution in the floor

layer. The stress deviator distribution is shown in Fig. 9.

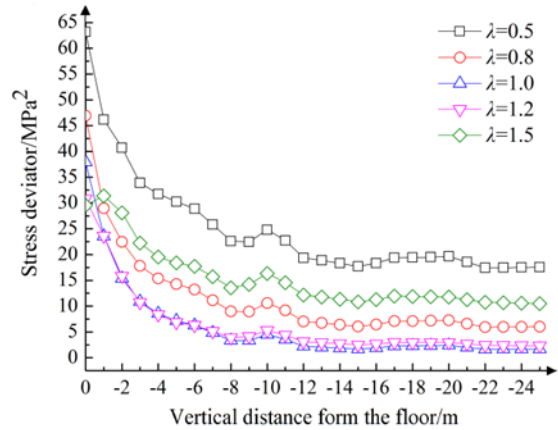
As shown in Fig. 9(a), when $\lambda = 0.5$, (1) the stress deviator does not change considerably below the floor of the goaf. At the position of $-5 \sim 0$ m from the coal side, the stress deviator increases rapidly and then decreases exponentially after reaching the peak. The rate of change in the stress deviator slows as the depth increases. (2) The peak values of the stress deviator at depths of $z = -5, -10, -15, -20$, and -25 m are 30.25, 24.81, 17.70, 19.65, and 17.11 MPa^2 , and the horizontal positions of the peak values in

each rock layer are $x = 3, 6, 8, 10$, and 11 m.

As shown in Fig. 9(b), when $\lambda = 1.0$, (1) the stress deviator in the surrounding rock below the floor does not change considerably. Then, it increases rapidly at a position of $-5 \sim 0$ m from the coal side. After reaching the peak value, the stress deviator decreases exponentially. The rate of change in the stress deviator decreases with increasing depth. (2) The peaks in the stress deviator are 7.19, 4.52, 1.67, 2.42, and 1.69 MPa^2 when the depth $z = -5, -10, -15, -20$, and -25 m, and the horizontal positions corresponding to

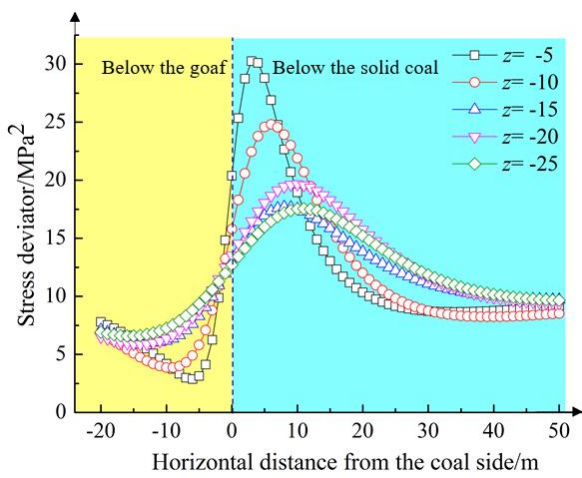


(a) Location of the peak stress deviator

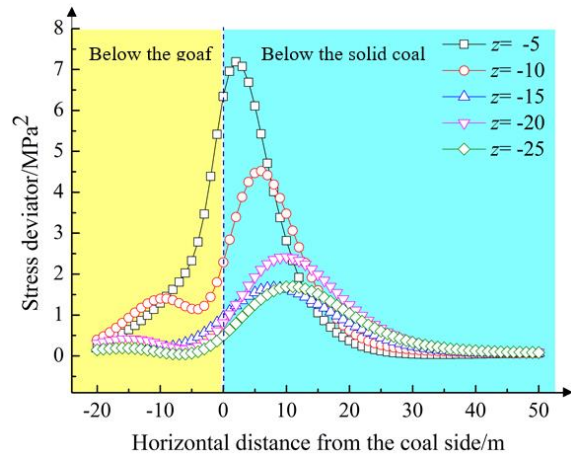


(b) The variation in the stress deviator along the peak axis

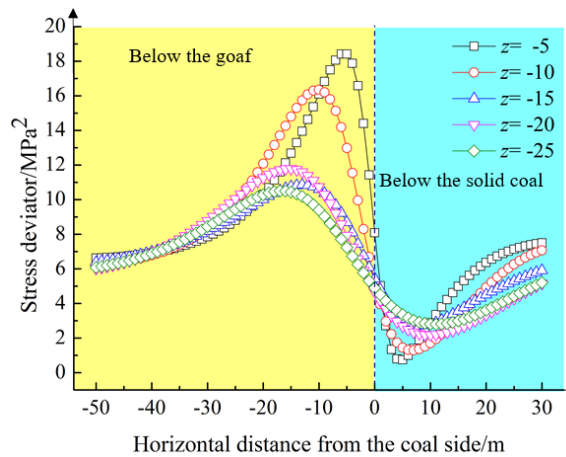
Fig. 8 Rotation of the stress deviator



(a) $\lambda=0.5$



(b) $\lambda=1.0$



(c) $\lambda=1.5$

Fig. 9 Stress deviator distribution at each depth

the peak values in each rock layer are $x = 2, 6, 8, 10,$ and 11 m.

Fig. 9(c) shows that when $\lambda = 1.5$, (1) the stress deviator in the rock layer below the floor begins to increase at a horizontal distance of $-30 \sim -20$ m from the coal side and gradually decreases after reaching the peak in the stress deviator. Then, the stress deviator increases again below the

solid coal. (2) The peaks of the stress deviator at depths $z = -5, -10, -15, -20,$ and -25 m are $18.41, 16.35, 10.85, 11.78,$ and 10.50 MPa^2 , and the horizontal positions corresponding to the peak values in each rock layer are $x = -5, -10, -13, -15,$ and -17 m.

Comparing Figs. 8 and 9 shows that the depth z and the horizontal stress coefficient λ will directly affect the

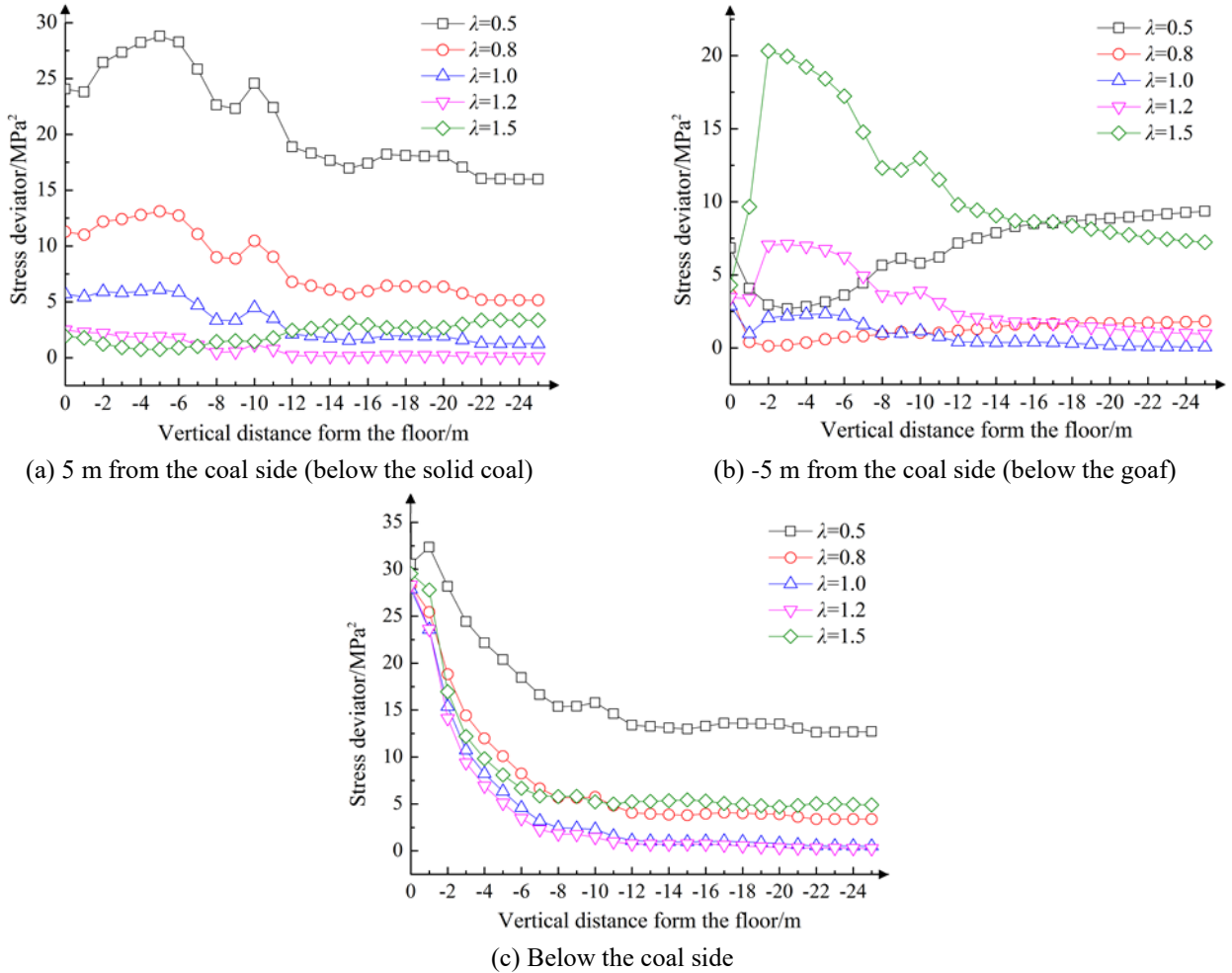


Fig. 10 Evolution of the stress deviator with depth

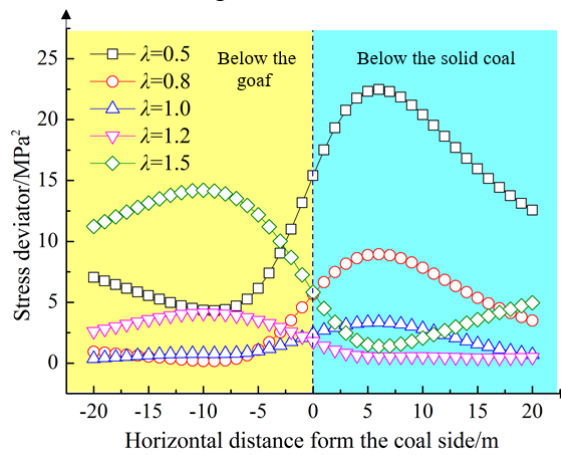


Fig. 11 Evolution of the stress deviator along the horizontal direction

magnitude and change rate of the stress deviator. The location of the stress deviator concentration area and the peak axis of the stress deviator are determined by the horizontal stress coefficient λ .

4.4 The vertical evolution of the stress deviator

The evolution curves of the stress deviator along the depth direction when $x = 5 \text{ m}$, -5 m and 0 m are shown in

Fig. 10 for different horizontal stress coefficients.

When $x=5 \text{ m}$, -5 m and 0 m , the surrounding rocks in the floor are located below the solid coal, below the goaf and below the coal side, respectively. The following findings are illustrated in Fig. 10:

(1) As shown in Fig. 10(a), for $\lambda \leq 1$, the curves of $\lambda = 0.5$ and 0.8 are taken as examples. The stress deviator in the surrounding rock below the solid coal increases from 24.06 and 11.28 MPa^2 to peaks of 28.79 and 13.10 MPa^2 as the

depth increases from 0 to 5–6 m, and then the stress deviator decreases at a slower rate of change while exhibiting a fluctuating trend. When $\lambda > 1$, the stress deviator remains essentially constant as the depth increases.

(2) As shown in Fig. 10(b), for $\lambda \geq 1$, the curves of $\lambda = 1.2$ and 1.5 are taken as examples. The stress deviator in the surrounding rock below the goaf increases from 3.46 and 4.30 MPa² to peaks of 7.08 and 20.32 MPa² as the depth increases from 0 to 2–3 m, and then the stress deviator gradually decreases. When $\lambda < 1$, the stress deviator slowly increases with increasing depth.

(3) As shown in Fig. 10(c), the stress deviator in the surrounding rock below the coal side decreases exponentially with increasing depth. As the depth increases from 0 to 10 m, the stress deviator decreases by 14.78, 22.51, 25.57, 26.87 and 24.33 MPa² when $\lambda = 0.5, 0.8, 1.0, 1.2,$ and 1.5, and the rates of change are high.

(4) Below a depth of 10 m, the variation in the stress deviator tends to be stable.

4.5 The horizontal evolution of the stress deviator

According to the geological situation of the Malan Mine, the floor of the #2 coal seam is located 9 m below the floor of the goaf. Therefore, the stress deviator of the rock layer at $z = -9$ m is selected as the research object, and its evolution along the horizontal direction is analyzed. The stress deviator distribution is shown in Fig. 11.

As shown in Fig. 11, at the same depth ($z = -9$ m), the stress deviator presents a single peak distribution for all of the constant λ values investigated.

(1) When $\lambda \leq 1$, taking $\lambda = 0.5$ and 0.8 as examples, the stress deviator changes only slightly below the goaf, increases sharply below the coal side, peaks at 6 m from the coal side, and then decreases rapidly. The maximum values of the stress deviator are 22.47 and 8.95 MPa² for $\lambda = 0.5$ and 0.8.

(2) When $\lambda > 1$, taking $\lambda = 1.2$ and 1.5 as examples, the stress deviator in the rock mass below the goaf peaks at -10 m from the coal side (with maximum values of 4.11 and 14.21 MPa²) and then gradually decrease, with only a slight change below the solid coal.

(3) When the horizontal distance from the coal side of the goaf exceeds 15 m, the stress deviator stabilizes.

5. Discussion

According to the data from the Malan Mine, the horizontal stress coefficient is $\lambda = 0.8$ in this area. Fig. 12 (a) and (b) show the distribution of the stress deviator below the 10606 goaf in the Malan Mine based on theoretical and numerical calculations. As shown in Fig. 12, the theoretical and numerical calculations of the stress deviator distribution are generally consistent, and the stress deviator concentration area is mainly located below the solid coal. The stress deviator below the goaf gradually decreases with increasing depth from the floor and generally decreases with increasing horizontal distance from the coal side; the smaller the depth, the higher the rate of stress deviator reduction. The peak axis of the stress deviator in both

figures is at an angle of approximately 30° to the vertical direction. The difference is that due to the idealized design of the mechanical model in the theoretical calculation, the theoretically calculated stress deviator distribution is more uniform and regular, and the range of the stress deviator concentration area is slightly larger.

As shown in Fig. 12, the #2 coal seam is located 7–9 m below the floor of the #02 coal seam (the dotted black line in the figure represents the roof and floor of the #2 coal seam). In the range of $z = -7$ m to $z = -9$ m, the stress deviator below the goaf changes drastically in the results of both the theoretical and numerical calculations. The stress deviator below the solid coal is very high, and the change rate is high, suggesting that this area is extremely unsuitable for a gas drainage roadway. Below the goaf, with an increase in the distance from the coal side, the stress deviator first decreases and then increases. In the theoretical calculation results, at $x = -11.5$ m, the stress deviator reaches the minimum value. In the numerical calculation results, when the roadway is located at $x = -10.2$ m, the stress deviator reaches the minimum value, and the change rate is low. Thus, this difference is very small. Considering that the theoretical calculation is relatively idealized, it is suggested that the 10608 gas drainage roadway in the #2 coal seam should be positioned at a horizontal distance of 10.2 m from the coal side.

To verify the scientific nature of the study, a rectangular roadway with cross-sectional dimensions of 4.0 m × 2.5 m was excavated in the #2 coal seam of the model. The horizontal distances from the roadway to the coal side were -15 m, -10 m, -5 m, 0 m, 5 m and 10 m. The vertical displacement of the roadway is shown in Fig. 13. This figure shows that when the horizontal distance between the roadway and coal side is -15 m, -10 m, -5 m, 0 m, 5 m and 10 m, the maximum deformation of the roadway roof is 12.3 mm, 11.5 mm, 13.5 mm, 20.8 mm, 25.2 mm and 24.7 mm, respectively.

As shown in Fig. 14, the maximum deformation of the roadway indicates that the deformation is large when the roadway is located below the coal side and solid coal. When the roadway is below the goaf, with the increase in the horizontal distance between the roadway and the coal side, the roadway deformation first decreases and then increases slightly. This result is consistent with the distribution of the stress deviator.

When studying the stress state of the surrounding rocks near the goaf, most research has focused on the vertical stress. When Xu *et al.* (2019) and Shang *et al.* (2019) studied the deformation and failure of near-goaf roadways, they focused on the vertical stress distribution near the goaf. Zhang *et al.* (2018) used vertical stress as an important reference in assessing the stability of surrounding rocks. In studies on closely spaced coal seam mining, the location of the roadway in the lower coal seam is also often based on the vertical stress distribution. Liu *et al.* (2016) determined the optimal position of a roadway in a lower coal seam through the study of the vertical stress and stress diffusion angle by numerical simulations. However, this method ignores the horizontal and shear stresses in the surrounding rock, and these factors have a great impact on the stability of the surrounding rock. The stress deviator is a

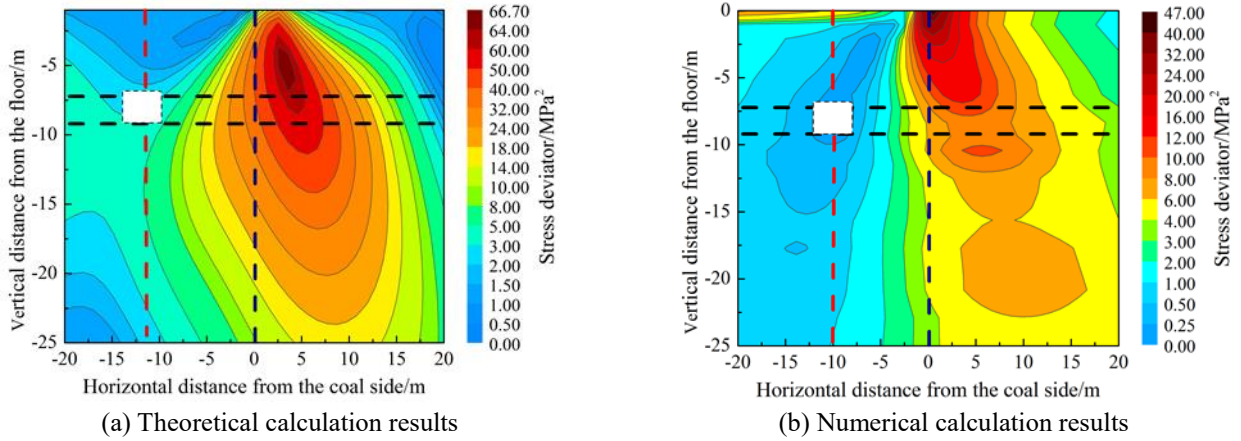


Fig. 12 Selection of roadway location

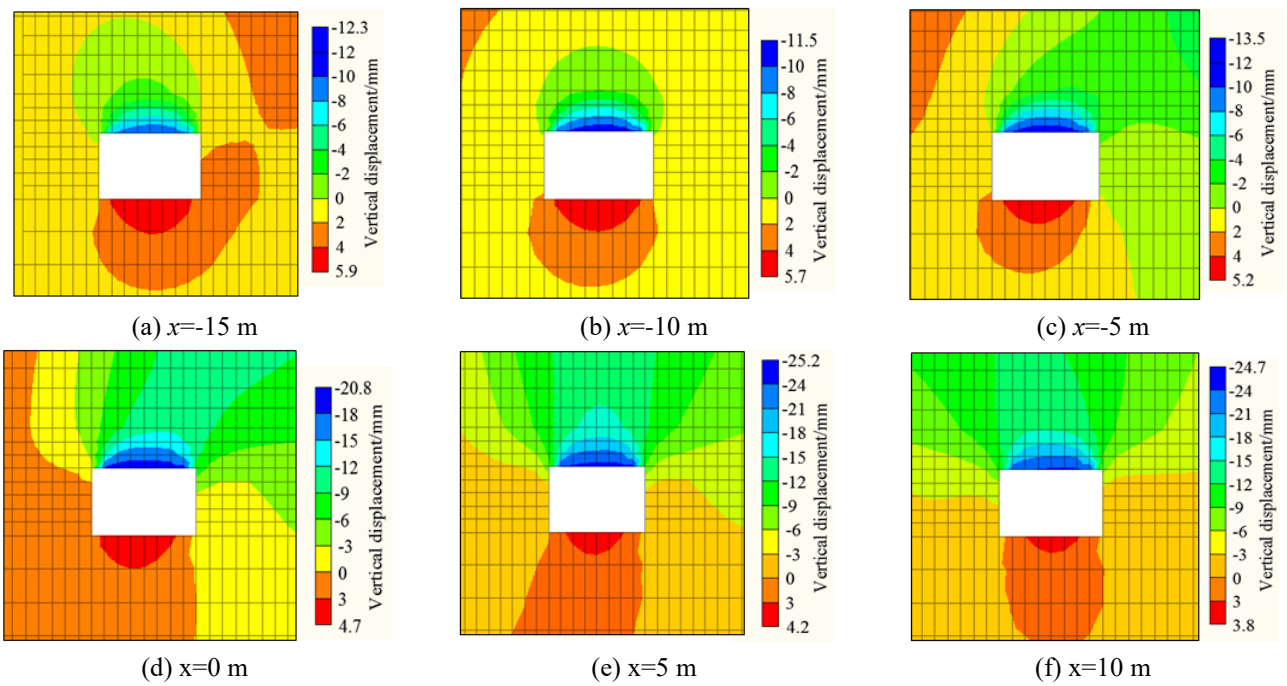


Fig. 13 The deformation of the roadway

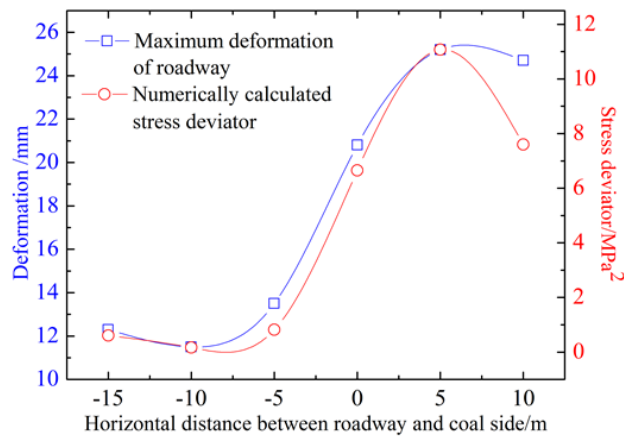


Fig. 14 Stress deviator and deformation of the roadway

comprehensive index that reflects the elastic-plastic state of the surrounding rocks, which should be valued. Zhang *et al.*

(2016) and Islam *et al.* (2009) analyzed the deviatoric stress around roadways and goafs, but those studies lack

theoretical calculations and analysis of the distribution of the stress deviator associated with a single goaf. In this paper, the theoretical formula of the stress deviator in the surrounding rock on one side of the goaf is deduced and calculated, and the distribution of the stress deviator with respect to different horizontal pressure coefficients is studied by combining theoretical calculations and numerical calculations. The results show that the magnitude of the stress deviator can accurately reflect the stability of the surrounding rock below a goaf and can provide a reasonable basis for planning the layout of roadways in the process of closely spaced coal seam mining.

In future research work, the stress deviator should be used as an evaluation criterion for the stability of surrounding rocks near mined-out areas. However, the study also has shortcomings. Due to the construction period, the scheme has not yet been implemented at the study site. In addition, the model in this paper is based on relatively simple engineering geological conditions. When studying the distribution of the stress deviator below a goaf with complex geological conditions (Nevitt *et al.* 2018, Sun *et al.* 2019), such as working faces with shallow burial depths below gully landforms or the presence of other large goafs or geological structures near the goaf (faults or collapsed columns), the changes in the stress distribution should be considered. Thus, the theoretical and numerical models in this paper should take into account all stress conditions, which will require further study.

6. Conclusions

(1) The expression of the stress deviator below the floor of a goaf is derived. The results of theoretical calculations and numerical simulations show that the stress deviator decreases exponentially from the rock mass below the coal side with increasing depth from the floor; as λ increases, the area of stress deviator concentration shifts, and the value of the stress deviator increases with the increase in $|\lambda|$.

(2) When $\lambda \leq 1$, the peak axis of the stress deviator is at an angle of 30° from the vertical direction; when $\lambda > 1$, the peak axis of the stress deviator is at an angle of -45° from the vertical direction. As the depth increases, the angle between the peak axis of the stress deviator and the vertical direction gradually decreases.

(3) As the depth increases below the solid coal, when $\lambda \leq 1$, the stress deviator decreases in a fluctuating manner. When $\lambda > 1$, the stress deviator remains basically unchanged. As the depth increases below the goaf, when $\lambda \geq 1$, the stress deviator increases rapidly and then decreases in a fluctuating manner. When $\lambda < 1$, the stress deviator slowly increases with depth; when the depth exceeds 10 m, the change in the stress deviator becomes stable.

(4) In a given horizontal plane, the stress deviator presents a single peak distribution. With an increase in λ , the peak position of the stress deviator shifts from the rock mass below the solid coal to the rock mass below the goaf. When the distance from the coal side exceeds 15 m, the variation in the stress deviator tends to be stable.

(5) Analysis of the stress deviator indicates that the reasonable horizontal distance of the 10608 gas drainage roadway from the coal side in the Malan Mine is 10.2 m.

The results of simulating the deformation of the roadway at various locations show the same results as the analysis of stress deviator. This finding suggests that the surrounding rock conditions are more favorable in places with lower stress deviator values.

Acknowledgments

The research described in this paper was financially supported by the Fundamental Research Funds for Central Universities of China University of Mining & Technology (Beijing) (CN) (2010YL09).

References

- Bernasconi, A. (2002), "Efficient algorithms for calculation of shear stress amplitude and amplitude of the second invariant of the stress deviator in fatigue criteria applications", *Int. J. Fatigue*, **24**(6), 649-657. [https://doi.org/10.1016/S0142-1123\(01\)00181-5](https://doi.org/10.1016/S0142-1123(01)00181-5).
- Brady, B.H. and Brown, E.T. (1993), *Rock Mechanics: for Underground Mining*, Springer Science & Business Media.
- Cao, Z., He, X., Wang, E. and Kong, B. (2018). "Protection scope and gas extraction of the low-protective layer in a thin coal seam: Lessons from the DaHe coalfield, China", *Geosci. J.*, **22**(3), 487-499. <https://doi.org/10.1007/s12303-017-0061-1>.
- Chen, M., Yang, S.Q., Zhang, Y.C. and Zang, C.W. (2016). "Analysis of the failure mechanism and support technology for the Dongtan deep coal roadway", *Geomech. Eng.*, **11**(3), 401-420. <https://doi.org/10.12989/gae.2016.11.3.401>.
- Chen, Y., Ma, S. and Cao, Q. (2018), "Extraction of the remnant coal pillar in regular and irregular shapes: A case study", *J. Loss Prevent. Process Industr.*, **55**, 191-203. <https://doi.org/10.1016/j.jlp.2018.06.012>.
- Cui, L. (2017). "Analysis on reasonable location and extraction effect of high-level gas drainage roadway in Malan Mine", *China Energy Environ. Protect.*, **39**(6), 132-136 (in Chinese).
- Das, A.J., Mandal, P.K., Paul, P.S. and Sinha, R.K. (2019), "Generalised analytical models for the strength of the inclined as well as the flat coal pillars using rock mass failure criterion", *Rock Mech. Rock Eng.*, **52**(10), 3921-3946. <https://doi.org/10.1007/s00603-019-01788-7>.
- Fu, J., Song, W.D. and Tan, Y.Y. (2018). "Study of stability and evolution indexes of gobs under unloading effect in the deep mines", *Geomech. Eng.*, **14**(5), 439-451. <https://doi.org/10.12989/gae.2018.14.5.439>.
- He, F., Xu, L., Wu, H.K. and Li, T.D. (2014), "Deviatoric stress transfer and stability of surrounding rock in large-section open-off cut roof", *Chin. J. Geotech. Eng.*, **36**(6), 1122-1128 (in Chinese). <https://doi.org/10.11779/CJGE201406018>.
- Islam, M.R., Hayashi, D. and Kamruzzaman, A.B.M. (2009). "Finite element modeling of stress distributions and problems for multi-slice longwall mining in Bangladesh, with special reference to the Barapukuria coal mine", *Int. J. Coal Geol.*, **78**(2), 91-109. <https://doi.org/10.1016/j.coal.2008.10.006>.
- Jaouhar, E.M., Li, L. and Aubertin, M. (2018), "An analytical solution for estimating the stresses in vertical backfilled stopes based on a circular arc distribution", *Geomech. Eng.*, **15**(3), 889-898. <https://doi.org/10.12989/gae.2018.15.3.889>.
- Jiang, Y. and Wang, Q. (2004), "J* integral of the specific deviator strain energy and its application", *Appl. Math. Mech.*, **25**(1), 110-122. <https://doi.org/10.1007/BF02437299>.
- Krause, E. (2009), "Systematisation of seams designed for

- extraction in mines from the aspect of the mining-geological and gas recognition level”, *Arch. Min. Sci.*, **54**(2), 203-222.
- Kroon, M. and Faleskog, J. (2013). “Numerical implementation of a J2 and J3 dependent plasticity model based on a spectral decomposition of the stress deviator”, *Comput. Mech.*, **52**(5), 1059-1070. <https://doi.org/10.1007/s00466-013-0863-6>.
- Li, Z.L., Dou, L.M., Cai, W., Wang, G.F., Ding, Y.L. and Kong, Y. (2016), “Roadway stagger layout for effective control of gob-side rock bursts in the longwall mining of a thick coal seam”, *Rock Mech. Rock Eng.*, **49**(2), 621-629. <https://doi.org/10.1007/s00603-015-0746-6>.
- Liu, X., Li, X. and Pan, W. (2016), “Analysis on the floor stress distribution and roadway position in the close distance coal seams”, *Arab. J. Geosci.*, **9**(2), 83. <https://doi.org/10.1007/s12517-015-2035-9>.
- Lockner, D.A. and Stanchits, S.A. (2002), “Undrained poroelastic response of sandstones to deviatoric stress change”, *J. Geophys. Res. Solid Earth*, **107**(B12), ETG-13. <https://doi.org/10.1029/2001JB001460>.
- Mahdevari, S., Haghghat, H.S. and Torabi, S.R. (2013), “A dynamically approach based on SVM algorithm for prediction of tunnel convergence during excavation”, *Tunn. Undergr. Sp. Technol.*, **38**, 59-68. <https://doi.org/10.1016/j.tust.2013.05.002>.
- Mahdevari, S., Shahriar, K. and Esfahanipour, A. (2014), “Human health and safety risks management in underground coal mines using fuzzy TOPSIS”, *Sci. Total Environ.*, **488**, 85-99. <https://doi.org/10.1016/j.scitotenv.2014.04.076>.
- Mahdevari, S., Shahriar, K., Sharifzadeh, M. and Tannant, D.D. (2017). “Stability prediction of gate roadways in longwall mining using artificial neural networks”, *Neur. Comput. Appl.*, **28**(11), 3537-3555. <https://doi.org/10.1007/s00521-016-2263-2>.
- Mahdevari, S., Shahriar, K., Sharifzadeh, M. and Tannant, D.D. (2016). “Assessment of failure mechanisms in deep longwall faces based on mining-induced seismicity”, *Arab. J. Geosci.*, **9**(18), 709. <https://doi.org/10.1007/s12517-016-2743-9>.
- Majcherczyk, T., Niedbalski, Z. and Małkowski, P. (2014), “Analysis of yielding steel arch support with rock bolts in mine roadways stability aspect”, *Arch. Min. Sci.*, **59**(3), 641-654. <https://doi.org/10.2478/amsc-2014-0045>.
- Marino, G.G. and Osouli, A. (2012), “Influence of softening on mine floor-bearing capacity: Case history”, *J. Geotech. Geoenviron. Eng.*, **138**(10), 1284-1297. [https://doi.org/10.1061/\(ASCE\)GT.1943-5606.0000693](https://doi.org/10.1061/(ASCE)GT.1943-5606.0000693).
- Nevitt, J.M. and Pollard, D.D. (2017), “Impacts of off fault plasticity on fault slip and interaction at the base of the seismogenic zone”, *Geophys. Res. Lett.*, **44**(4), 1714-1723. <https://doi.org/10.1002/2016GL071688>.
- Shan, R., Kong, X. and Yu, Z. (2013), “Theory and application of strong support for coal roadway sidewall”, *Chin. J. Rock Mech. Eng.*, **32**(7), 1304-1314 (in Chinese).
- Shang, H., Ning, J., Hu, S., Yang, S. and Qiu, P. (2019), “Field and numerical investigations of gateroad system failure under an irregular residual coal pillar in close-distance coal seams”, *Energy Sci. Eng.*, **7**(6), 2720-2740. <https://doi.org/10.1002/ese3.455>.
- Singh, A.K., Singh, R., Maiti, J., Kumar, R. and Mandal, P.K. (2011), “Assessment of mining induced stress development over coal pillars during depillaring”, *Int. J. Rock Mech. Min. Sci.*, **48**(5), 805-818. <https://doi.org/10.1016/j.ijrmm.2011.04.004>.
- Sivakugan, N., Widisinghe, S. and Wang, V.Z. (2014), “Vertical stress determination within backfilled mine stopes”, *Int. J. Geomech.*, **14**(5), 06014011. [https://doi.org/10.1061/\(ASCE\)GM.1943-5622.0000367](https://doi.org/10.1061/(ASCE)GM.1943-5622.0000367).
- Suchowerska, A.M., Merifield, R.S. and Carter, J.P. (2013), “Vertical stress changes in multi-seam mining under supercritical longwall panels”, *Int. J. Rock Mech. Min. Sci.*, **61**, 306-320. <https://doi.org/10.1016/j.ijrmm.2013.02.009>.
- Sun, J., Wang, L. and Zhao, G. (2019), “Stress distribution and failure characteristics for workface floor of a tilted coal seam”, *KSCE J. Civ. Eng.*, **23**(9), 3793-3806. <https://doi.org/10.1007/s12205-019-0786-7>.
- Sun, J., Wang, L. and Zhao, G. (2019), “Stress distribution and failure characteristics for workface floor of a tilted coal seam”, *KSCE J. Civ. Eng.*, **23**(9), 3793-3806. <https://doi.org/10.1007/s12205-019-0786-7>.
- Sun, Y.J., Xie, S.R., Li, S.J., Song, B.H. and Huang, X. (2016), “Reasonable location of roadway in coal pillar area under different layer-located key blocks and its surrounding rock control”, *J. China Univ. Min. Technol.*, **45**(4), 694-701 (in Chinese). <https://doi.org/10.13247/j.cnki.jcmt.000550>.
- Tan, Y.L., Zhao, T.B. and Xiao, Y.X. (2010). “In situ investigations of failure zone of floor strata in mining close distance coal seams”, *Int. J. Rock Mech. Min. Sci.*, **47**(5), 865-870. <https://doi.org/10.1016/j.ijrmm.2009.12.016>.
- Toraño, J., Diez, R.R., Cid, J.R. and Barciella, M.C. (2002), “FEM modeling of roadways driven in a fractured rock mass under a longwall influence”, *Comput. Geotech.*, **29**(6), 411-431. [https://doi.org/10.1016/S0266-352X\(02\)00006-X](https://doi.org/10.1016/S0266-352X(02)00006-X).
- Wang, H., Zhao, Y.X., Mu, Z.L., Jiao, Z.H., Zhang, X. and Lu, Z.G. (2017), “The mechanism of rockburst in district coal pillar with high stress deviator and mining tremors impact and its prevention methods”, *J. China Univ. Min. Technol.*, **46**(6), 1202-1212 (in Chinese). <https://doi.org/10.13247/j.cnki.jcmt.000729>.
- Wang, Z.J., Luo, Y.S., Guo, H. and Tian, H. (2012), “Effects of initial deviatoric stress ratios on dynamic shear modulus and damping ratio of undisturbed loess in China”, *Eng. Geol.*, **143**, 43-50. <https://doi.org/10.1016/j.enggeo.2012.06.009>.
- Widisinghe, S. and Sivakugan, N. (2014), “Vertical stress isobars for trenches and mine stopes containing granular backfills”, *Int. J. Geomech.*, **14**(2), 313-318. <https://doi.org/10.12989/gae.2018.15.3.889>.
- Xu, Y., Pan, K. and Zhang, H. (2019), “Investigation of key techniques on floor roadway support under the impacts of superimposed mining: Theoretical analysis and field study”, *Environ. Earth Sci.*, **78**(15), 436. <https://doi.org/10.1007/s12665-019-8431-9>.
- Yan, H., Weng, M.Y., Feng, R.M. and Li, W.K. (2015), “Layout and support design of a coal roadway in ultra-close multiple-seams”, *J. Central South Univ.*, **22**(11), 4385-4395. <https://doi.org/10.1007/s11771-015-2987-7>.
- Yavuz, H. (2004), “An estimation method for cover pressure re-establishment distance and pressure distribution in the goaf of longwall coal mines”, *Int. J. Rock Mech. Min. Sci.*, **41**(2), 193-205. [https://doi.org/10.1016/S1365-1609\(03\)00082-0](https://doi.org/10.1016/S1365-1609(03)00082-0).
- Yuan, H.H., Shan, R.L. and Su, X.G. (2018), “Deformation characteristics and stability control of a gateroad in fully mechanized mining with large mining height”, *Arab. J. Geosci.*, **11**(24), 767. <https://doi.org/10.1007/s12517-018-4087-0>.
- Zhang, M. and Zhang, Y. (2018), “Stability evaluation method for gateways in closely spaced coal seams and surrounding rock control technology”, *Arab. J. Sci. Eng.*, **43**(10), 5469-5485. <https://doi.org/10.1007/s13369-018-3201-7>.
- Zhang, W., Zhang, D., Qi, D., Hu, W., He, Z. and Zhang, W. (2018), “Floor failure depth of upper coal seam during close coal seams mining and its novel detection method”, *Energy Explor. Exploit.*, **36**(5), 1265-1278. <https://doi.org/10.1177/0144598717747622>.
- Zhang, G. and He, F. (2016), “Asymmetric failure and control measures of large cross-section entry roof with strong mining disturbance and fully-mechanized caving mining”, *Chin. J. Rock Mech. Eng.*, **35**(4), 806-818 (in Chinese). <https://doi.org/10.13722/j.cnki.jrme.2015.0917>.
- Zhao, C., Hebblewhite, B.K. and Galvin, J.M. (2000), “Analytical

solutions for mining induced horizontal stress in floors of coal mining panels”, *Comput. Meth. Appl. Mech. Eng.*, **184**(1), 125-142. [https://doi.org/10.1016/S0045-7825\(99\)00097-3](https://doi.org/10.1016/S0045-7825(99)00097-3).

Zhao, Z., Deng, G., Han, Y., Zhang, Z., Dong, Y. and Gao, Y. (2020), “Comparison of deformation behavior of saturated sand under constant and variable deviatoric stress”, *KSCE J. Civ. Eng.*, **24**(3), 762-769. <https://doi.org/10.1007/s12205-020-0976-3>.

Zhu, S., Lu, L., Wu, Y. and Zhang, T. (2017), “Comprehensive study on the deformation and failure characteristics of a mining-impacted deep double-longwall working face floor”, *J. Geophys. Eng.*, **14**(3), 641-653. <https://doi.org/10.1088/1742-2140/aa64aa>.

CC